CERN – EUROPEAN ORGANIZATION FOR NUCLEAR RESEARCH
European Laboratory for Particle Physics

CTF3 Note 054 (MD)
(Preliminary Phase)

Report on the Third Operation of the CTF3 Preliminary Phase in 2002, 16 September - 25 October

R. Corsini, L. Rinolfi, F. Tecker, CERN, Geneva
A. Ferrari (Ed.), Department of Radiation Sciences, Uppsala University
P. Royer, Institut de Physique des Hautes Energies, Université de Lausanne
C. Biscari, A. Gallo, A. Ghigo, INFN-LNF, Frascati

Abstract

In this note, we report on the third (and last) operation period of the CTF3 Preliminary Phase in 2002. After installation of new RF deflectors in the isochronous ring and after optimization of the optics, the bunch train combination was successfully demonstrated with a factor four and five. The combination performance was tested, in terms of bunch length and of bunch-to-bunch variations in intensity, as well as in transverse and longitudinal positions. Finally, the new Uppsala bunch frequency monitor was commissioned.

Geneva, Switzerland
28 February, 2003

1 Introduction

The main goals for this third and last operation period of 2002 were to improve the bunch train combination scheme after installation of new RF deflectors developed by INFN Frascati and to commission a new beam monitor developed by Uppsala University. After optimization of the optics, and in particular of the ring orbits, we managed to combine properly four and five bunch trains. Signals coming out from the Uppsala monitor were recorded and analysed both in the time domain and in the frequency domain.

2 The Bunch Train Combination Experiment

2.1 Installation of the new RF deflectors and first operation with beam

The CTF3 complex was opened on August 26 for the installation of new transverse RF deflectors. These RF cavities were designed and build by INFN-Frascati as prototypes to be used in the combiner ring of the CTF3 nominal phase. Their main advantage with respect to the previous ones is the increased aperture (43 mm instead of 21 mm). They are 10 cell travelling wave structures with a negative group velocity and a $2\pi/3$ phase advance per cell, and they require a power of 6.6 MW each for the nominal deflection angle of 4.5 mrad at a beam energy of 350 MeV.

These new RF deflectors were installed at the location of the ones that had been used before. Since they are longer than the previous RF deflectors, the adjacent quadrupole magnets (HR.QFN64 and HR.QFN91) had to be moved upstream by 30 cm each. This also required the two bumpers (i.e. the dipole correctors that create a closed bump at the injection septum) to be taken out from the ring. The deflectors were connected to the temperature regulating water circuit and to the RF network fed by the modulator-klystron WL.MDK33. The RF conditioning went smoothly and a power of 26 MW was finally obtained at the klystron exit for a 2.3 μs pulse at a rate of 25 Hz. This means that a power of more than 10 MW has been provided to each deflector.

When operation with beam started again (using the fast kicker for injection), the advantage of the larger deflector aperture was clear. Beam losses were reduced right away and it was possible to change the beam orbit over a large range, by varying the injection conditions (i.e. the fast kicker amplitude and the currents of the septum and of the horizontal corrector HIE.DHZ23), without affecting the losses over the first few turns. The bunch train combination process was first tested with the new RF deflectors on September 27, using the settings that were obtained during the previous operation period for a combination factor four [1]. It was observed that the first pulse from the gun had a higher charge than the following ones. Since its energy was also somewhat higher because of beam-loading in the linac, it was decided to suppress this first pulse during the first turn in the ring by firing the fast kicker HR.KFI91 together with the RF deflector. The possibility of kicking out also the second pulse was originally foreseen. This has been performed experimentally, but we noticed that the energy difference between the second pulse and the following ones was very small and well within the ring acceptance. Therefore, for the sake of simplicity, only the first pulse was kicked out during standard operating conditions. The combination was then performed with the following four pulses, with an efficiency larger than 80%.

2.2 Determination of the closed orbit and RF injection

The increase of the acceptance due to the larger deflector aperture made it easier to define and implement a procedure for the setting-up of the bunch train combination process, which will be described later on.

A necessary pre-requisite for this setting-up procedure is a good knowledge of the ring closed orbit. A measurement of the closed orbit has already been performed by using standard techniques [2, 3], which require to operate in the accumulation mode. However, in order to take into account the difference between the isochronous optics and the accumulation optics, a new procedure has been tested.

The beam is injected using the fast kicker. After optimising the settings of the septum and of the kicker in order not to have any loss in the ring, the beam position is recorded in the UMAs of the ring, over several turns (typically 10). An average position is then computed for each UMA, and this is assumed to describe the closed orbit. This technique allows to get rid of possible coherent betatron oscillations and non-periodic dispersion components resulting from injection errors, by averaging them over many turns. The beam energy can be varied during this procedure, and its final value is chosen such as to minimize the displacements due to the periodic dispersion in the ring. In the end, the closed orbit is validated by re-optimizing the injection parameters and by observing that the beam keeps the same position in each UMA over several turns.

It must be noted that it is also possible to use the first RF deflector HR.SDH91 instead of the fast kicker in order to inject one pulse only in the ring. The pulse can then be left circulating over several turns. This relies on the fact that the timing and the length of the RF pulse from the modulator-klystron WL.MDK33 which powers the deflectors can be adjusted so that the first deflector provides a kick during a period which is long enough to inject the 6.6 ns long electron pulse, but no RF power reaches both deflectors by the time the pulse has completed its first turn, i.e. 420 ns later. The beam then does not receive any kick during the following turns. The nominal RF pulse length used to inject and combine up to five pulses is of the order of 2.7 μs. For RF injection of one electron pulse only, the RF pulse length is reduced down to approximately 50 ns. Since the kicker and the deflector are not at the same position, the phase advance between the septum and the deflector is slightly different from the one between the septum and the kicker. The septum settings therefore must be changed in order to follow the closed orbit, when going from kicker injection to RF deflector injection.

Figure 1 shows the case of an injection with the RF deflector HR.SDH91, where the beam stays in the ring for 27 turns before being extracted. The signal is very similar to the one obtained when injecting the beam with the fast kicker. In particular, after optimization, there are almost no losses. This is the demonstration that the new RF deflectors are perfectly suitable for the injection of a bunched beam into a ring.

2.3 Procedure for the bunch train combination

The following procedure allows to determine experimentally the five free parameters which are relevant for the combination process: the RF phase and power in each deflector, and the RF frequency.

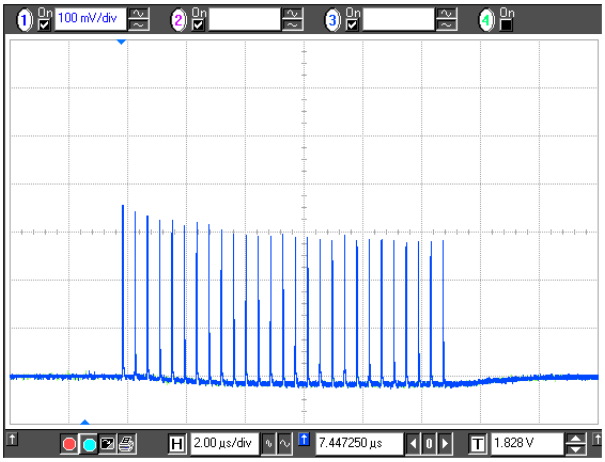

Figure 1: Beam injection in the ring with one RF deflector. The signal of the beam position monitor (UMA) shows that the beam is injected and stays in the ring during 27 turns (before being extracted) with almost no losses. Note that the baseline is lower under the beam pulses.

The RF network associated with the deflecting structures is shown in Figure 2. The first RF deflector seen by the beam coming from the injection line and used for the injection is HR.SDH91, and the second RF deflector is HR.SDH71. The modulator-klystron WL.MDK33 powers both deflectors. After the power splitter, there is a phase shifter and a power attenuator on the waveguide which is connected to HR.SDH71. The phase and the power in HR.SDH91, which is used for injection, are therefore determined by the phase and power controls of the klystron, whereas the phase shifter and the power attenuator provide two independent knobs allowing control of the phase and the power in the second cavity HR.SDH71. Tuning the power in the second cavity is necessary in order to obtain equal kick strengths in the two deflectors, because the length of the RF waveguides between the modulator-klystron WL.MDK33 and each deflector is not the same, resulting thus in different power losses.

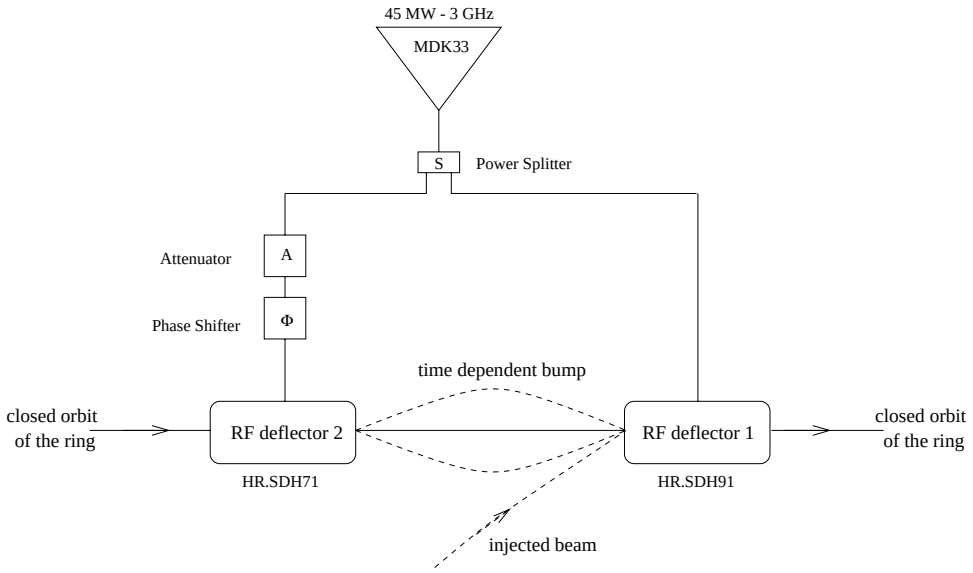

Figure 2: Schematic RF network associated with the RF deflecting structures.

The procedure which is detailed in the following refers to a multiplication factor of four. In this case, the procedure is simplified because after one turn, the beam arrives at the zero crossing of the deflecting field in the second RF deflector and it is therefore not deflected. This procedure is based on the use of only one pulse from the gun. Once it is completed, the four pulses are sent in the machine for the combination.

Initially, the RF deflector HR.SDH91 is used in order to inject the beam on the previously measured closed orbit. The modulator is thus switched on and the fast kicker is disabled. The attenuation on the waveguide going to the second deflector is set to its maximum value so that no power reaches the second cavity HR.SDH71, and there is no kick. Alternatively, as described before, the RF pulse length and timing can be adjusted such that no RF power is present in the second cavity HR.SDH71 when the beam passes through it.

– Phase in HR.SDH91: The phase of the klystron is varied step by step while monitoring the horizontal beam position in HR.UMA91, which is located downstream of the deflecting structure. The horizontal position of the beam describes a cosine curve corresponding to the RF field in the cavity, and the phase corresponding to the crest can easily be identified. Figure 3 shows a phase scan as observed in HR.UMA91.

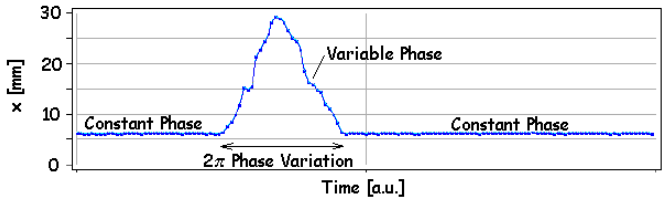

Figure 3: Determination of the RF phase in the injection deflector HR.SDH91 by looking at the signal in HR.UMA91. The horizontal beam position is measured while changing the RF phase in the deflector by 2π. The minimum position of the beam with respect to the centre of the vacuum chamber ($x = 0$) corresponds to the injected beam on the crest of the field.

– Amplitude in HR.SDH91: The kick amplitude must be such that the beam is injected on the closed orbit of the ring. The power at the output of the klystron is therefore varied until the beam passes in the UMAs at the same positions as for the closed orbit. Figure 4 shows the mean trajectory which defines the closed orbit and the trajectory at the first turn when using the RF deflector for injection.

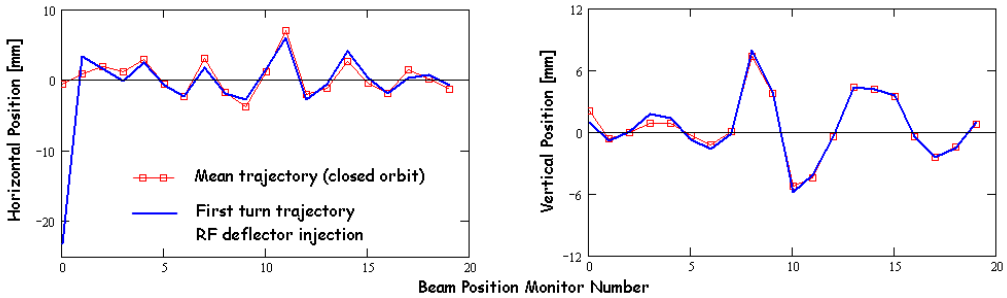

Figure 4: Reference closed orbit and first turn trajectory in the isochronous ring in both planes. The reading in the first UMA shows the beam position at injection, before the deflector kick.

– At this point, the frequency f_0 of the whole CTF3 complex must be tuned to satisfy the relationship between the ring circumference C and the multiplication factor N, i.e. $C = n\lambda_0 \pm \lambda_0/N$, where n is an integer. This is done by looking at the second turn in the ring with only HR.SDH91 in operation. After one turn, for a combination factor of four, the bunches must arrive in the deflector at the zero-crossing of the RF field, such that they are not deflected. The frequency of the whole complex is therefore tuned around the nominal frequency of 2.998550 GHz so that, after going through the active deflector HR.SDH91, the second turn orbit is the same as at the first turn. This indicates that the frequency is adapted to the length of the orbit for the combination factor of four.

At the end of this operation, the frequency of the whole complex, as well as the phase and the power in the first RF deflector HR.SDH91 (controlled by the phase and the power of the modulator-klystron WL.MDK33), are fixed. It is now possible to find the phase and the amplitude in the second RF deflector HR.SDH71 in order to obtain a closed bump between the deflectors.

– Phase in HR.SDH71: In the case of a multiplication factor of four, after one turn in the ring, the injected bunches must also arrive in the second RF deflector HR.SDH71 at the zero crossing of the RF field. The attenuation is thus set to its minimum value so that the second RF deflecting cavity is fed by the maximum available power. The phase shifter which controls the phase in HR.SDH71 is then varied until the beam does not experience any deflection in HR.SDH71 at the second turn and therefore follows the closed orbit. A difference in the kick amplitudes of the two deflectors is not important at this stage. On the contrary, having the maximum available power in HR.SDH71 enhances the sensitivity to the phase.

– Amplitude in HR.SDH71: After two turns in the ring, the bunches arrive in HR.SDH71 on the crest, with the opposite kick sign compared to the injection. At this point, they are deflected by HR.SDH71 away from the septum and the injection deflector HR.SDH91 must close the bump. The only remaining free parameter is the amplitude in HR.SDH71 which must be varied by tuning the power attenuator at the entrance of HR.SDH71. The closed bump is achieved when the beam follows the closed orbit in the ring (outside the injection region) during the third turn, after the bump.

It must be noted that one or two iterations of the procedure can be necessary to achieve the best optimisation since, for instance, tuning the frequency of the complex can induce small changes in the RF phase of the klystron, which then needs to be optimised again. Once this procedure is finished, it is then possible to inject four pulses in the ring, as required for the combination.

2.4 Deflector bump amplitude at the third turn

The procedure which we described in the previous section was systematically applied and the losses could be reduced. However, it was not possible to bring them down to zero, and some problems were put in evidence. In particular, some beam losses were apparent at the third turn, when the electron pulse must follow a closed bump, that brings it away from the septum in the region between the two deflectors. Evidently, part of the beam was hitting the outer side of the vacuum chamber. The vacuum chamber is indeed not symmetrical around the ideal beam axis

in this region, leaving only about a 58 mm clearance on the outer side, while the distance from the axis of the injected beam is about 73 mm. Without the bumpers, the position of the central orbit can not be easily changed. In order to solve the problem, a number of measures had to be taken:

– The ring optics was slightly changed in order to decrease the horizontal β-function in the injection region, and the beam was transversally re-matched. The observation of the beam on the screen HR.MTV82 confirmed that a smaller beam size was obtained, although the transverse matching was probably not perfect yet.

– It was also observed that the measured closed orbit was displaced towards the outer part of the ring between the deflectors. By using the horizontal correctors HR.DHZ61, HR.DHZ91 and HR.DHZ35, it was possible to displace the closed orbit towards the septum, gaining more beam clearance. However, the amplitude of the closed orbit oscillations with respect to the ideal machine center was somewhat increased.

2.5 Deflector bump closure

After the implementation of the new optics, of the re-matching and of the closed orbit displacement, the losses at the third turn were reduced to zero. However, it was still not possible to exactly close the bump. Hence, this issue had to be studied in more detail.

The effect of a single kick $\Delta x'$ at a location s_0 on the closed orbit at any location s is given by:

$$\Delta x(s) = \frac{\sqrt{\beta(s_0)\cdot\beta(s)}\ \cos(|\mu(s)-\mu(s_0)|-\pi Q)}{2\ \sin(\pi Q)}\cdot\ \Delta x'(s_0) \qquad (1)$$

In this equation, β and μ are respectively the beta-function and the phase advance in the considered transverse direction, and Q is the tune. For the contributions of two kicks (coming from the two RF deflectors in this case) to cancel, the phase advance between these two kicks has to be a multiple of π and the terms $\sqrt{\beta(s_i)}\cdot\Delta x'(s_i)$ (s_i being the location of the kick, $i=1,2$) have to be equal.

The ring optics had to be modified when installing the new RF deflectors: since they are longer than the previous ones, two quadrupoles (HR.QFN64 and HR.QFN91) were displaced by 30 cm. This resulted also in the loss of the ring symmetry around the centre of the long straight sections, i.e. the injection and extraction regions. The optics was optimized in order to improve the injection efficiency. With the settings used for the combination, the MAD model actually predicts a phase advance of 1.14 π between the two RF deflectors. In addition, the beta-function at HR.SDH91 is larger than at HR.SDH71, which means that a stronger kick is needed in HR.SDH71 in order to close the bump. The RF powers on the two deflectors was measured by RF specialists and were found to be equal in the case where a maximum RF power is sent into HR.SDH71. Since an attenuator (HR.SDH71-ATTN) is installed upstream of HR.SDH71, only a further attenuation is possible there. As a result, a bump closure is impossible. Figure 5 shows the MAD simulation for the closed orbit in this case.

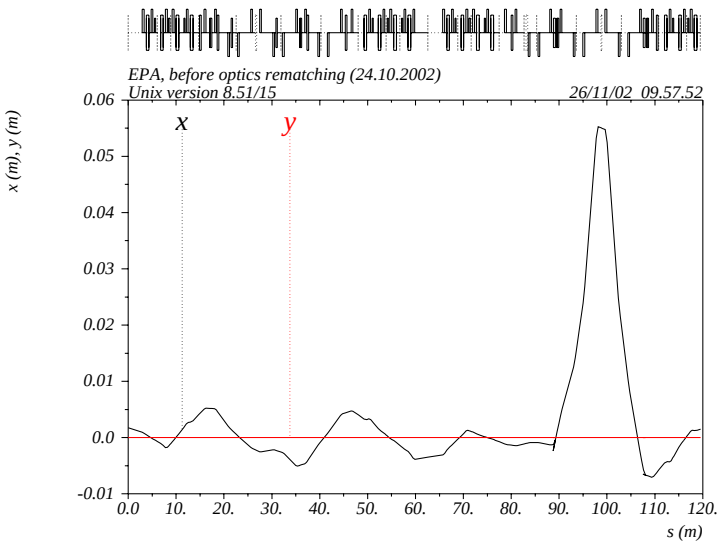

Figure 5: Closed orbit in the ring with a deflection of 4 mrad in both RF deflectors.

In a next step, the optics was re-matched with MAD in order to achive a phase advance of π between the deflectors. Additionally, the beta-function at HR.SDH91 was chosen to be smaller than at HR.SDH71. Therefore, a weaker kick is needed at HR.SDH71, which is always possible to achieve when using the attenuator. Figure 6 shows the MAD simulation in this case.

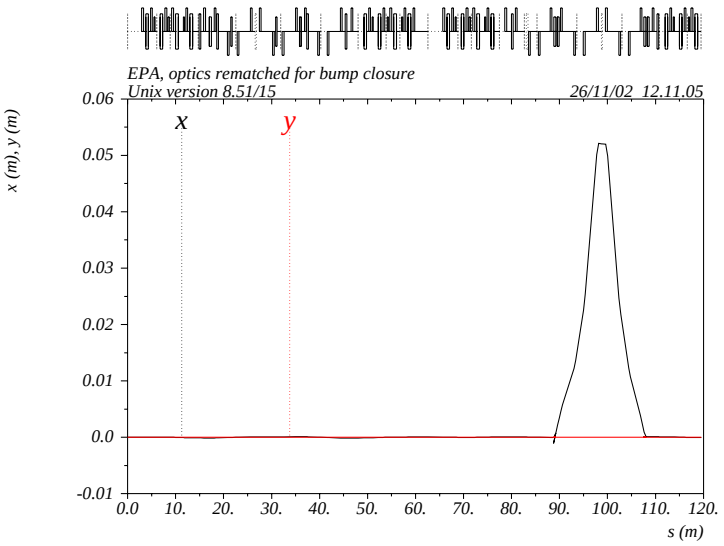

Figure 6: Closed orbit in the ring with a deflection of 4 mrad in HR.SDH91 and 95% of this in HR.SDH71.

A phase and amplitude scan was performed on HR.SDH71-PHAS and HR.SDH71-ATTN in order to vary the power in HR.SDH71. With the optimal settings, the trajectory difference measured between the second and third turns was only 0.3 mm rms. This is of the same order of magnitude as the reproducibility of the measurement. Therefore, we managed to obtain a perfect bump closure, as it is shown in Figure 7.

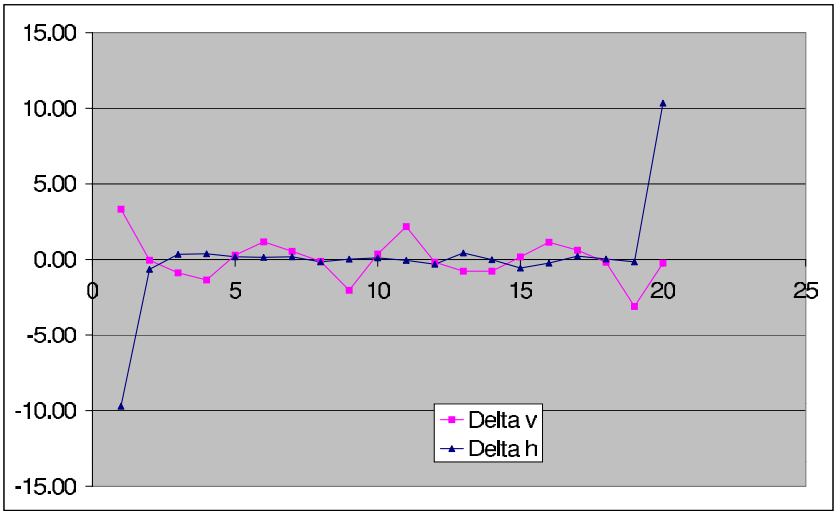

Figure 7: Trajectory difference (in mm) between the second and third turns, as measured by the 20 beam position monitors along the ring. The first and last UMAs in the graph show a large horizontal difference because of the different position inside the RF deflector bump for the various turns. The rms value is 0.3 mm in the rest of the ring.

2.6 Bunch train combination results, with various combination factors

After having performed the optimization described previously, the results of the bunch train combination were excellent, showing a 100% combination efficiency. The charge multiplication could be observed on the UMAs of the ring. Figure 8 shows that the charge recorded by HR.UMA11 increases linearly turn after turn. It corresponds to a case with no losses.

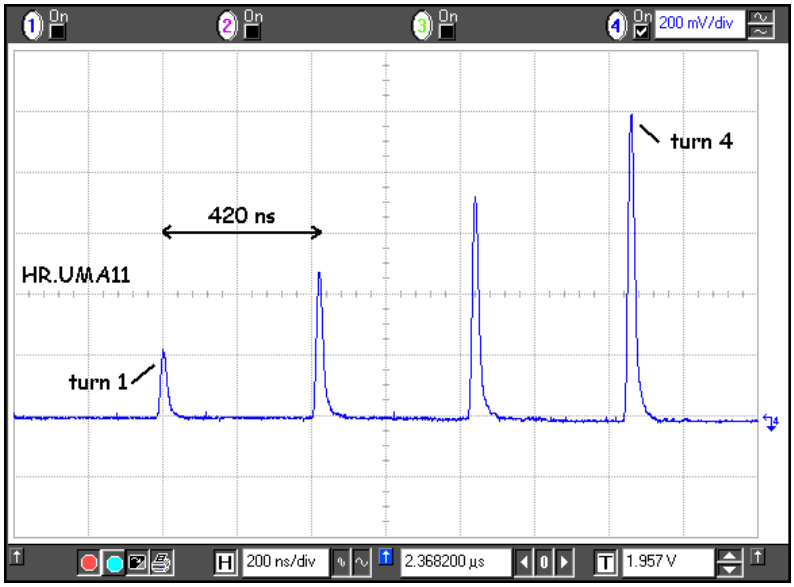

Figure 8: Bunch train combination with a factor four, as observed in the beam position monitor HR.UMA11 in the ring. The charge increases of the same amount at each turn, as a new train of bunches is combined with those circulating in the ring. After four turns, the pulse charge is multiplied by four.

The evolution of the time structure of the electron pulse was observed with the streak camera. Figure 9 shows the streak camera pictures and the corresponding intensity profiles, observed in the synchrotron light port HR.MSR58. The images are taken during the fourth turn in the ring, with an intermediate sweep speed in the streak camera. They show bunches located at the centre of the 6.6 ns pulse.

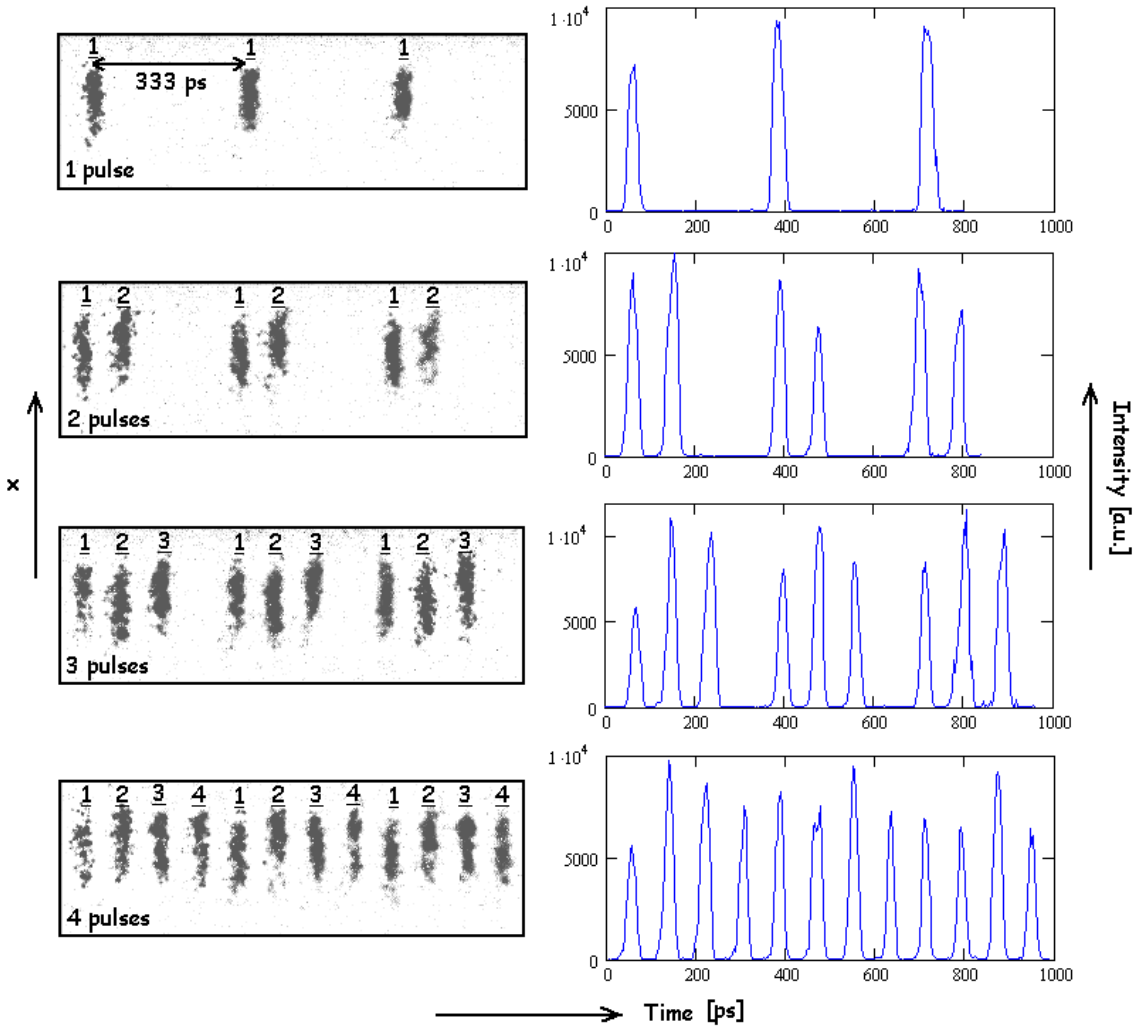

Figure 9: Bunch train combination with a factor four: streak camera images (left column) and corresponding intensity profiles (right column). All images are taken during the fourth turn. Each line corresponds to one additional pulse coming out of the gun, starting with one pulse (top) and ending with four pulses (bottom). The numbers above the bunches refer to the pulse number to which they belong.

In the standard operating conditions, the power required in order to inject the beam using the RF deflector HR.SDH91 is about 18 MW at the output of the modulator-klystron. Taking into account the power splitter which divides the power by a factor two, and also assuming a standard attenuation of 0.02 dB/m in the 50 m long waveguide between the modulator-klystron WL.MDK33 and the deflector HR.SDH91, this corresponds to a power of 7.2 MW at the cavity input, which is in very good agreement with the expectations.

The bunch train combination with a factor five was experimented as well. As already mentioned, the exact frequency of the linac and of the RF deflectors corresponding to a combination factor four was experimentally determined during the setting-up procedure: we obtained $f_4 = 2.998585$ GHz $\pm$ 10 kHz, which is very close to the expected nominal frequency (the error on the frequency corresponds to the small frequency changes made on different days while optimising the combination). Such a frequency corresponds to a ring orbit length of 125.647 m $\pm$ 0.5 mm, calculated using the relationship between the frequency f_N and the ring orbit length C, for a bunch frequency multiplication factor N:

$$C = \frac{\beta c}{f_N}\left(1257 - \frac{1}{N}\right) \tag{2}$$

where βc is the velocity of the electrons.

The circumference which is measured here corresponds exactly to the design value of 125.647 m. However, it is not compatible with the orbit length measured when operating the ring in accumulation mode, which was about 9 mm shorter [3]. This difference is not well understood yet, but it could result from the fact that the closed orbits in the two modes were different, since the optics and the settings of the corrector dipoles were not the same.

The change in the RF frequency needed for a combination factor five was derived from the previous equation, and then re-tuned experimentally. We obtained $f_5 = 2.998715$ GHz $\pm$ 10 kHz. This increase of the frequency was followed by a decrease of the cooling water temperature of all RF structures (including the accelerating sections), in order to avoid perturbation of their resonant properties. Also, for the combination factor five, a 100% efficiency was obtained. In Figures 10 and 11, the evolution of the beam current and of the time structure of the electron pulse during combination are shown.

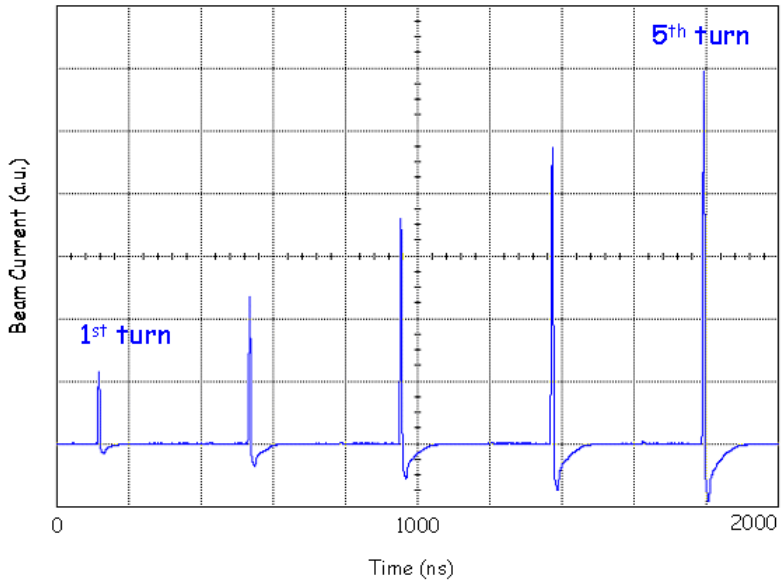

Figure 10: Bunch train combination with a factor five, as seen on the wide-band beam pick-up HR.UMA62WB in the ring.

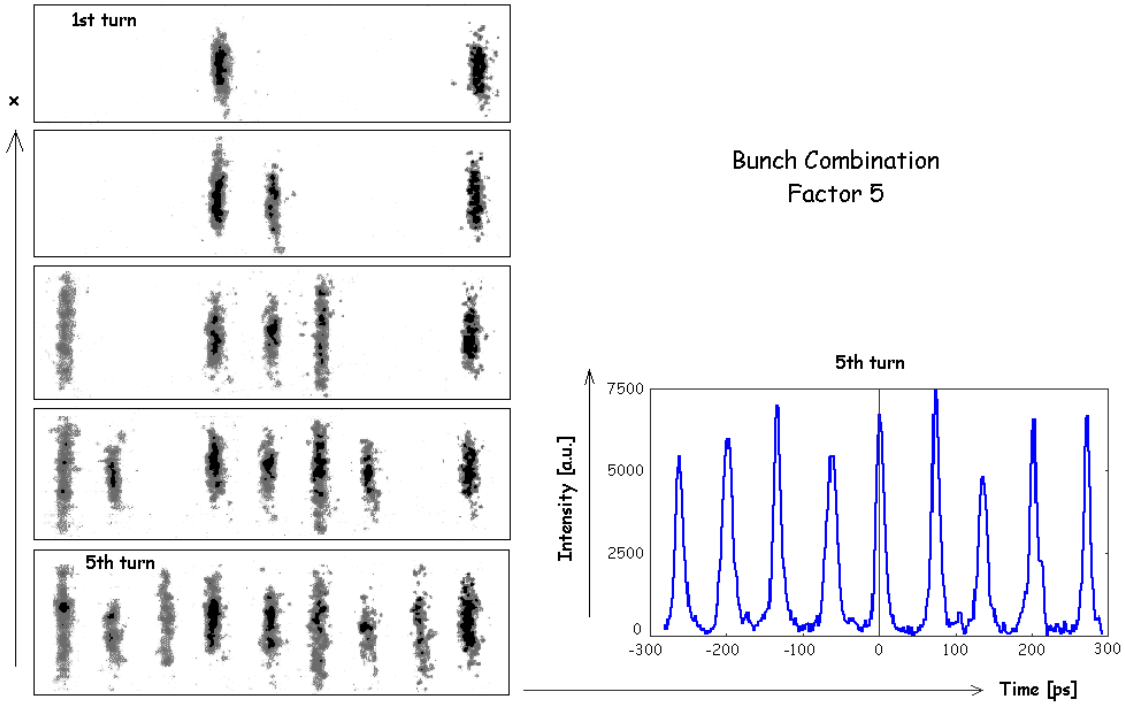

Figure 11: Bunch train combination with a factor five: streak camera images (left) and intensity profile after combination (right).

2.7 Combination performances

In this section, we discuss the performances of the bunch train combination process. As pointed out previously, we managed to combine four or five pulses without losses. However, other conditions should also be satisfied to use the combined pulse for efficient production of high frequency RF power, as planned in the CTF3 nominal phase. Although the pulse current in the preliminary phase is too low for RF power production, the measurement of the combined pulse characteristics was considered as a fundamental issue in order to understand the potential limitations of the process. The important parameters to be measured are listed below:

- Bunch Length: The bunch extension must be short with respect to the RF wavelength. Bunch lengthening in the injection line and in the ring must remain minimal.

- Bunch-to-bunch intensity variations. In order to obtain a good flat-top in the RF pulse, the current along the combined pulse must be constant. Bunch-to-bunch charge variations can also indicate losses.

- Bunch-to-bunch variations in transverse position. The aim of the bunch train combination is to put the pulses onto the same orbit. Variations in tranverse position are equivalent to an effective emittance growth. They can complicate the transport of the beam after its extraction from the ring and give rise to transverse instabilities.

- Bunch-to-bunch distance variations. The distance between two consecutive bunches after the combination must be constant and equal to the RF wavelength to be produced (or an integer multiple of it). Variations will cause a loss of efficiency.

All of these quantities were studied by analysing the synchrotron radiation emitted in the ring, with the streak camera. The synchrotron light set-up in the ring is shown in Figure 12. Three synchrotron light ports (HR.MSR52, HR.MSR56 and HR.MSR58) are available in the bending magnets of the fourth arc of the CTF3 ring, from the injection point. These ports are located at three positions with different values of the dispersion, covering the range from almost a zero dispersion (HR.MSR58) to the maximum absolute value of 3 m (HR.MSR52). Movable mirrors are used to select the particular source to be observed. An optical arrangement transports the light to the streak camera laboratory, which is located in a separated room.

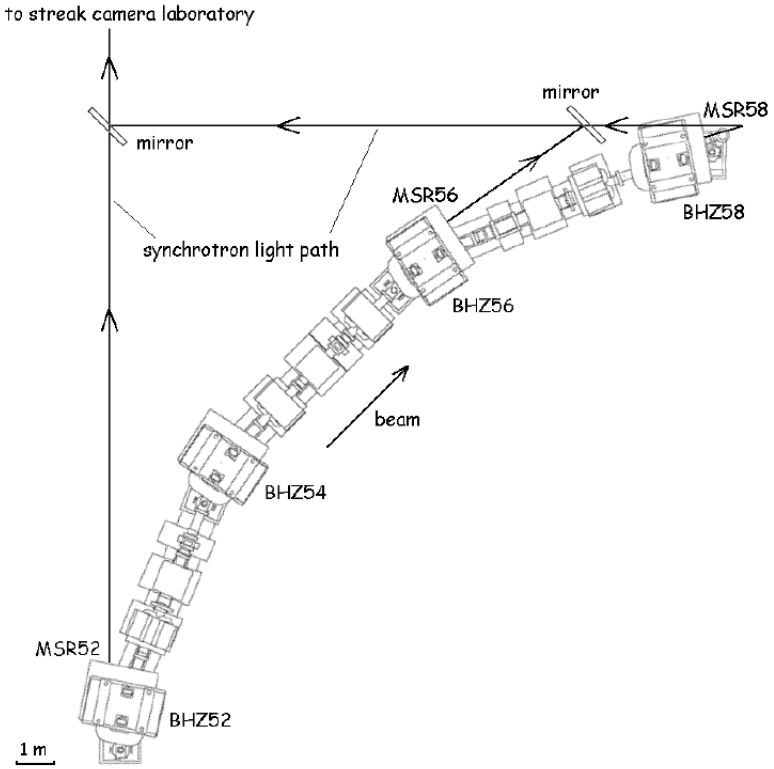

Figure 12: Synchrotron light ports (HR.MSR52, HR.MSR56 and HR.MSR58) in the fourth arc of the ring. The synchrotron light is brought from the ring level to the ceiling level and then transported to the streak camera laboratory through lenses and mirrors. The lenses along the optical path are not shown.

2.7.1 Bunch length measurements

The apparent bunch length seen on the streak camera images depends on the aperture of the slit at the entrance of the streak camera, and on the possible use of an optical filter to correct the chromatic effects of the optical lines transporting the synchrotron light to the streak camera. As an example, Figures 13 and 14 show two images of a combination with a factor four, taken with and without a 500 ± 20 nm passband filter, and observed during the fourth turn in the synchrotron light port HR.MSR52. When using the optical filter, the typical length measured on the streak camera profiles during the combination is of the order of 4-5 ps rms. These values do not change over several turns and are comparable with the ones obtained at the end of the

linac, also with the optical filter. The same bunches were observed without any optical filter and then have an apparent length of 9 ps rms. The difference is mainly due to the chromatic effects in the optical system (mirrors, lenses) transporting the light from the synchrotron light port to the streak camera. In any case, the precision in the bunch length measurement with the streak camera is limited by the intrinsic resolution of the streak camera which is about 3 ps rms. Within this limitation, no bunch lengthening either in the injection line or in the ring was observed.

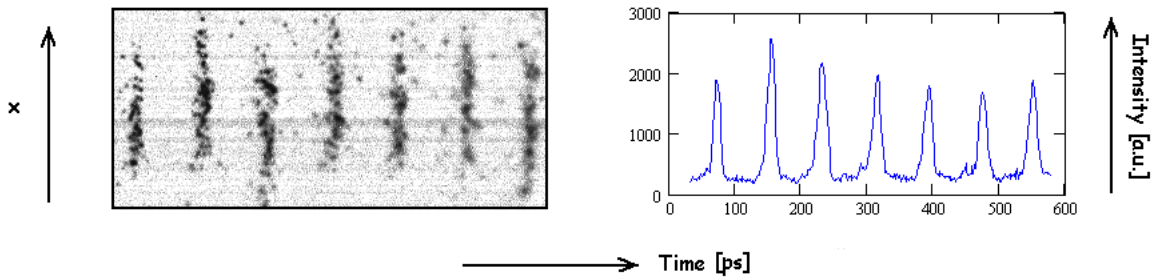

Figure 13: Bunch train combination with a factor four, as observed through a 500 nm optical filter. The apparent bunch length is of the order of 5.5 ps rms.

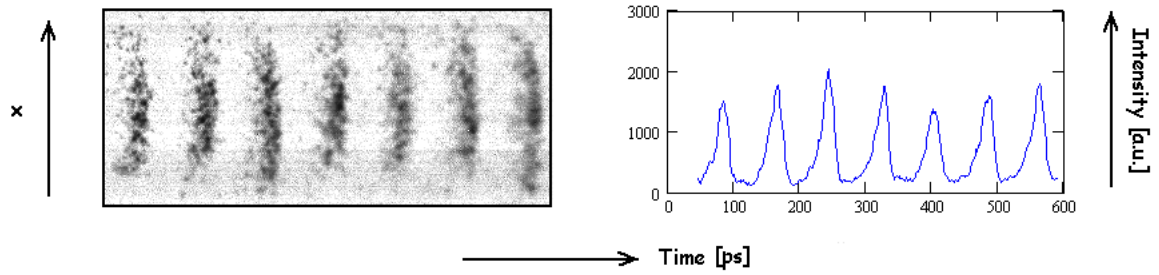

Figure 14: Bunch train combination with a factor four, as observed without any optical filter. The apparent bunch length is of the order of 9 ps rms.

2.7.2 Bunch-to-bunch variations in intensity

When looking at the intensity profiles of the different bunches (see Figures 9 and 11), some variations can be observed in the light intensity received by the streak camera. These variations do not result from beam losses, which were not occuring within the precision of the UMA measurements. The light intensity variations can have two main origins. First, subsequent bunches belong to different pulses, and the combination process is therefore sensitive to pulse-to-pulse variations. Indeed, pulse-to-pulse variations in charge, length and longitudinal profile were observed in the linac both using the beam position monitors and the screen WL.TCM37 in conjunction with the streak camera. These variations originated from the gun pulser, and were roughly non-systematic. After the combination, they also result in light intensity variations. These effects are minimum in the centre of the 6.6 ns long pulse, where the best overlap between the combined pulses is achieved. It must be noted that in this last operation period, because of time limitations, we used the spare pulser only, which is known to have limited performances

in stability. The pulser for the CTF3 nominal phase has been specified and designed for much more stable conditions. Secondly, the horizontal and vertical positions of the beam fluctuate in the machine if the orbits are not exactly the same at each turn. This results in a displacement of the synchrotron light source, and hence light intensity variations due to losses in the optical lines. This second effect could be minimised after optimization.

2.7.3 Bunch-to-bunch variations in transverse position

Figure 15 shows a streak camera image of a bunch train combination with a factor five, as observed during the fifth turn in the synchrotron light port HR.MSR56. The vertical axis of the streak camera images is the horizontal coordinate of the bunches in the ring and it is therefore also related to the dispersion function. Figure 15 shows that the electron bunches have different horizontal positions, but also that bunches belonging to the same pulse have the same position. This phenomenon has two main sources.

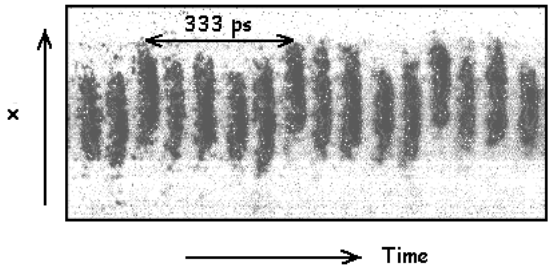

Figure 15: Bunch train combination with a factor five.

The first source for this effect is the small differences in the energy of the pulses used for the combination. These pulse-to-pulse energy variations arise during acceleration, either from the beam-loading in the linac structures, or from small variations in amplitude and phase along the RF pulse. These energy variations are transformed into position variations because of the non-zero dispersion at the observation point. This was experimentally confirmed by observing different position variations depending on the synchrotron light port which was used. These variations are more important in HR.MSR52 and HR.MSR56, where the dispersion is larger. For instance, in HR.MSR52 where $|D| \simeq 3$ m, a relative energy variation of $\Delta p/p = 0.1\%$ corresponds approximately to a transverse displacement of 3 mm. On the other hand, these variations vanish in regions with zero dispersion and, therefore, they do not correspond to an increase of the transverse emittance.

The second source for the bunch-to-bunch variations in position is an injection error (in position and/or angle). The injected pulse orbit then oscillates from turn to turn around the closed orbit and the horizontal position of the bunches at the observation point varies from turn to turn. Therefore, since different pulses reach the observation point after a different number of turns, their bunch position appears to be different in the streak camera image. This phenomenon is equivalent to a transverse emittance growth. However, it was mainly observed during the first combination experiments, before the optimisation procedure consisting in minimising the turn-to-turn orbit differences was systematically applied. The orbit difference that was obtained then (see section 2.5) is smaller than the average horizontal beam size σ_{h}, which is about 0.5 mm.

2.7.4 Bunch-to-bunch variations in longitudinal position

Figure 16 shows a streak camera image of a bunch train combination with a factor five, as observed during the fifth turn in the synchrotron light port HR.MSR56. The bunch spacing, which should be close to 67 ps is clearly not constant at that point. This image was taken before the injection optimization.

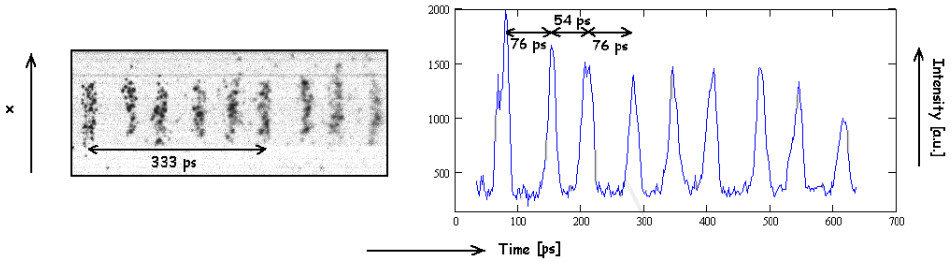

Figure 16: Bunch train combination with a factor five showing bunch spacing variations. Here, the correct bunch spacing should be $333/5 \simeq 67$ ps.

Since the precision of the bunch spacing after the bunch combination is a crucial issue for the CLIC drive beam scheme, a specific experiment was carried out to measure the bunch spacing variations and compare them with the expectations from the model of the ring. Two pulses were injected and combined in the ring, and the bunch spacing was observed turn after turn, from the second to the fifth turn. This was first done with an optimised injection. Then, the current in the septum magnet was changed (by about 0.1%), causing an injection mismatch. Figure 17 shows two streak camera images of the bunches observed during the second and third turns in the case of an injection mismatch. The bunch spacing indeed varies from 50 ps at the second turn to 85 ps at the third turn, whereas it should be close to 67 ps and constant for a combination factor of five.

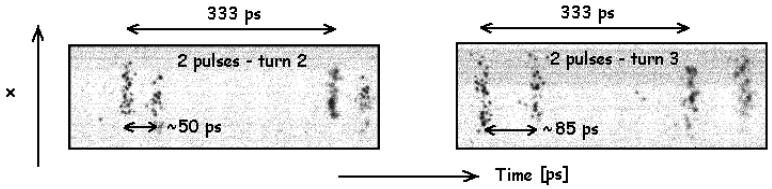

Figure 17: Turn-to-turn bunch spacing variations during the combination of two pulses with injection errors. The bunch spacing varies from 50 ps at the second turn (left) to 85 ps at the third turn (right).

The bunch-to-bunch distance variations were therefore linked to errors at the injection. An explanation of the effect is given below. The distance between two consecutive bunches is closely related to the isochronicity of the ring. Although the isochronicity condition simplifies to a zero momentum compaction factor in the case of achromatic lattices and ultra-relativistic electrons, the most general condition corresponds to a vanishing variation of the time of flight between particles, which is expressed by:

$$\left(\frac{1}{L}\int_{\mathcal{L}}\frac{C(s)}{\rho(s)}\mathrm{d}s\right)x_0+\left(\frac{1}{L}\int_{\mathcal{L}}\frac{S(s)}{\rho(s)}\mathrm{d}s\right)x_0'+\left(\alpha_c-\frac{1}{\gamma^2}\right)\frac{\Delta p}{p}=0 \qquad \forall\, x_0, x_0', \frac{\Delta p}{p}. \tag{3}$$

This condition includes two integrals multiplied by the initial conditions x_0 and x'_0 of the beam in the horizontal plane (in the case of horizontal curvature only). In the case of achromatic lattices where $D = D' = 0$ at the observation point, the integrals evaluated over one turn vanish and the isochronicity is reduced to $\alpha_c - 1/\gamma^2 = 0$. In the opposite case, where $D \neq 0$ and $D' \neq 0$ at the observation point, the integrals evaluated over one turn are not zero. The diagnostic tool used to monitor the bunch spacing is the streak camera set-up which uses the synchrotron light emitted in bending magnets (see Figure 12), where the dispersion is different from zero. During the first combination experiments, the injection process was not optimised, resulting in pulses oscillating around the closed orbit. The orbits were therefore different turn after turn, which implied different conditions x_0 and x'_0 at the observation point for each turn. According to equation (3) with non-zero integrals, the orbit variations were then transformed into variations in the time of flight of the particles in the bunches. This delay in the time of flight was visible in the streak camera during the combination, for which subsequent bunches travel a different number of turns.

The values of the integrals in equation (3) are in fact two elements of the transfer matrix of the ring, evaluated at the observation point for one turn, and can thus easily be calculated. By adjusting the two free parameters x_0 and x'_0, corresponding to the injection errors, it was indeed possible to reproduce the variations in the bunch spacing at the observation point.

Figure 18 shows a comparison between the measurements and the model predictions for the bunch spacing observed in HR.MSR52 and HR.MSR56 for large injection errors. For each turn, 15 streak camera images are recorded, and the error bars on the measured bunch spacing show the extreme measured values. The solid curves were obtained by using the ring transfer matrix given by the model and the values $x_0 = 0.8$ mm, $x'_0 = 0.6$ mrad which are adjusted in order to correspond to the measurements in HR.MSR56. For the same initial conditions, the model therefore predicts the bunch spacing at the location of HR.MSR52, thus showing that the mechanism leading to the variable spacing is well understood.

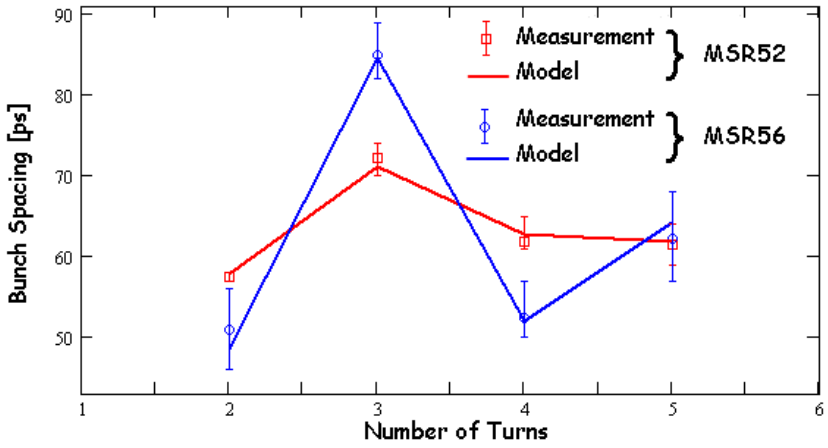

Figure 18: Bunch spacing variations after the combination of two pulses as a function of the number of turns observed from the synchrotron light ports HR.MSR52 (squares) and HR.MSR56 (circles) in the case of large injection errors. The solid curves correspond to the model predictions in both cases.

Figure 19 shows a comparison between the measurements and the model predictions for the bunch spacing in HR.MSR56 as a function of the number of turns in the case of small and large injection errors. The solid curves are obtained in the same way as before, with the same values of x_0 and x'_0 in the case of large injection errors, and with $x_0 = -0.2$ mm, $x'_0 = 0.2$ mrad in the case of the optimised injection. Both cases show a very good agreement between the model and the measurements. In addition, the optimised case shows that it is possible to reduce the variations to a very low level (i.e. 2 ps peak-to-peak, within the measurement resolution) by minimising the injection errors.

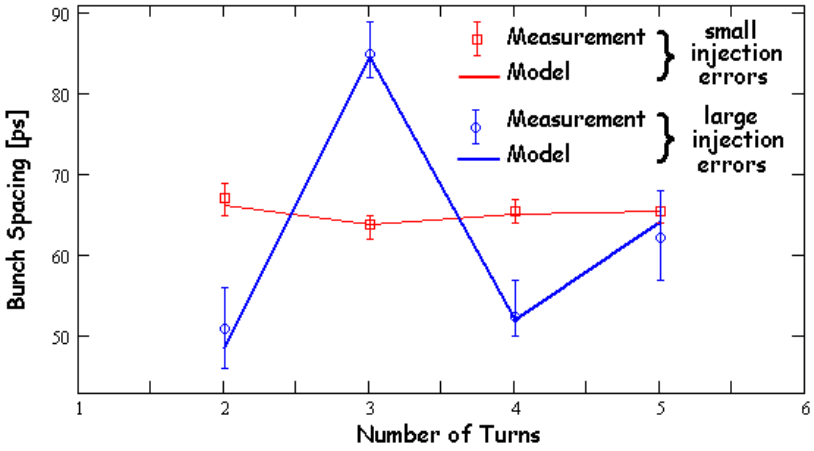

Figure 19: Bunch spacing variations after the combination of two pulses as a function of the number of turns for large (circles) and small (squares) errors at injection. The solid curves correspond to the model predictions in both cases.

In conclusion, the variations of the bunch spacing observed on the streak camera images after the combination are understood and explained by the non-achromatic lattice at the streak camera observation point. By definition, this effect is dependent on the observation point. In the injection (or ejection) region of the ring, where the achromatic condition is true, the correct bunch spacing is restored independently of the orbit errors.

This was confirmed by an independent experiment. An electron pulse was injected in the ring by the fast kicker, and the injection orbit was optimized. The timing of the RF pulse from the modulator-klystron WL.MDK33 was then adjusted in order to power the deflector HR.SDH71 only at the second turn in the ring. The phase shifter was then set such that the beam passed at the zero-crossing of the RF amplitude (no deflection). Then, the current in the corrector HR.DHZ91 was varied in order to induce strong beam oscillations, with amplitudes that were similar to the ones of the two-pulse experiment. We observed that the beam position, as recorded in the pick-up HR.UMA73 at the second turn, was not affected by the kick in the RF deflector HR.SDH71 (the beam position was the same, within 0.5 mm, with and without RF power in the deflector). Therefore, we concluded that the pulse arrived in HR.SDH71 always at the zero-crossing, independently on its orbit. The maximum orbit length variation was estimated by comparing the difference in position (0.5 mm) and the maximum deflection at the pick-up HR.UMA73 (± 17.5 mm), and it was found to be smaller than 2 ps.

3 Commissioning of the Uppsala bunch frequency monitor

A streak camera was generally used to visualize the longitudinal structure of the pulses and to monitor the interleaving of the bunches during the operation of the CTF3 preliminary phase. However, an alternative method, based on frequency spectrum analysis, was also tested during this operation period. When the first pulse is injected into the EPA isochronous ring, the distance between two consecutive bunches is 10 cm, i.e. 333 ps. Therefore, all harmonics of 3 GHz can be found in the beam power spectrum. After the bunch train combination, the distance between two consecutive bunches is reduced by a factor four or five and, as a result, only the harmonics of respectively 12 or 15 GHz should be found in the beam power spectrum. More details on this issue can be found in [4]. In that reference, the preliminary design of a coaxial extraction pick-up was also performed with MAFIA [5]. Later, the design of this pick-up evolved in order to include a miniature ultrahigh vacuum feedthrough [6] while meeting various technical constraints. The final geometry of the RF pick-up is shown in Figure 20.

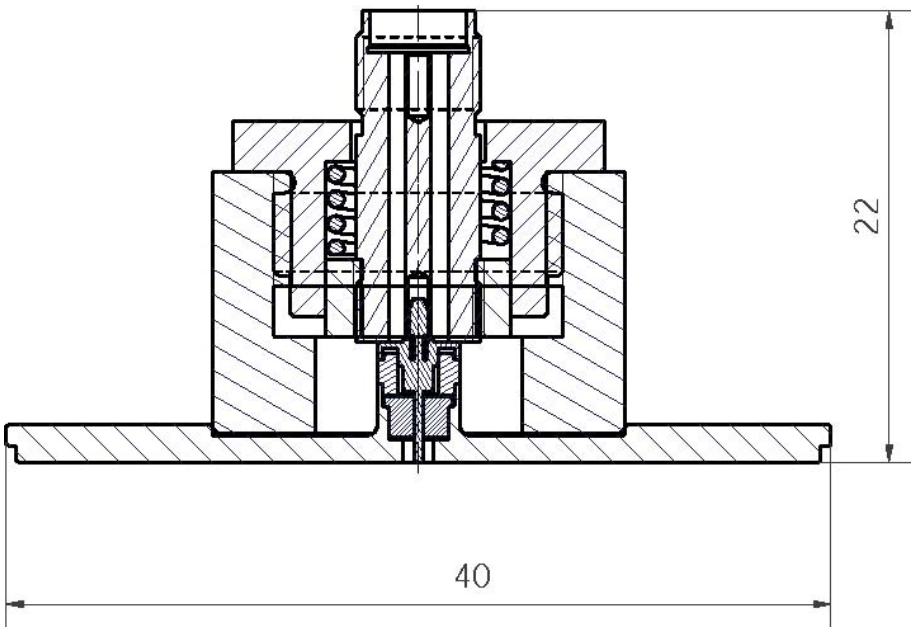

Figure 20: Technical drawing of the coaxial RF pick-up (the dimensions are in mm).

The RF pick-up signal is transported to a detection system. There, the signal first goes through a wideband amplifier and a 10 dB attenuator and it is then divided in five channels, by using two power splitters. Each channel is then terminated by a bandpass filter which selects the harmonic of interest. Afterwards, each signal is sent through a low noise amplifier. Each of the detection lines is terminated by a detector diode, which measures the amplitude of the incoming RF wave. The signals are extracted from the detection system through SMA-BNC connectors and they are then transported to a fast multi-channel digital oscilloscope for further analysis. A general layout of the detection system is shown in Figure 21. While assembling the detection system at Uppsala University, we measured its frequency response with a network analyzer. For each of the five channels, it was checked that the transmission for the harmonic of interest was at least 30 dB larger than for the other harmonics of 3 GHz. The response of the detector diodes was also studied: no variation of their response with the input frequency was observed.

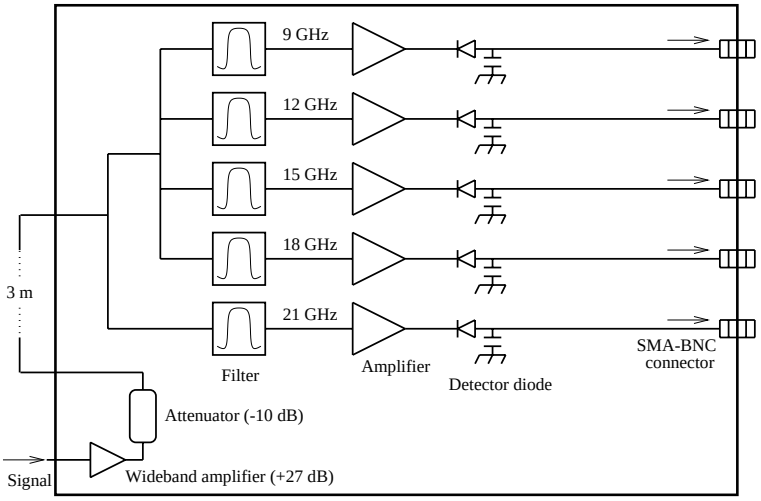

Figure 21: Layout of the detection system.

The Uppsala bunch frequency monitor HR.PHM60 was mounted in the ring in September 2002, at the exit of the HR.BHZ58 bending magnet. Before starting measurements with beam, calibration tests were performed in order to determine the amplitude response at each frequency of interest. It was checked that a large range of input powers could be covered, from -30 dBm up to 0 dBm. By driving an RF synthetizer operating at a fixed frequency with a DC pulse generator, we could generate very short RF signals (less than 10 ns), that were then injected into the detection system. When doing this, we noticed that the maximum amplitude of the output signal on the oscilloscope was strongly dependent on the length of the RF pulse at the input of the detection system. In particular, if the length of the input RF pulse is of the order of a few ns, the detection system does not reach a steady state and the maximum amplitude of the output signal is therefore much smaller than what it would be with a long input RF pulse. This is illustrated in Figure 22, which shows the response of the 15 GHz channel to an input RF pulse with an amplitude of -15 dBm and with two different lengths.

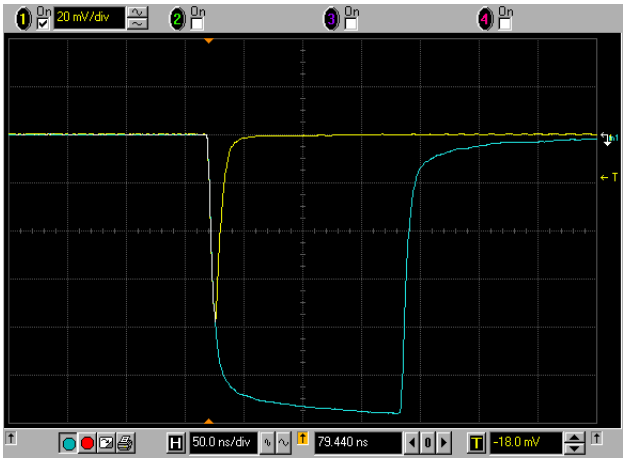

Figure 22: Response of the 15 GHz channel to RF pulses with the same amplitude of -15 dBm and with two different lengths: the short pulse is less than 10 ns long, while the long pulse is about 150 ns long. The fall time and the rise time of the measured signals are the same in both cases. No reflections are observed.

The short length of the bunch trains is one major limitation for the commissioning of HR.PHM60 during the operation of the CTF3 preliminary phase, since it does not allow an absolute measurement of the amplitude of the signals coming out from the RF pick-up. An accurate calibration of the detection system is therefore difficult, because of the uncertainties related to the shape and the length of the bunch trains circulating in the ring. However, in the future stages of the CTF3 project, the expected length for the electron bunch trains is 140 ns. The measurement of the power coming from the RF pick-up will then be much easier, since the detection system can reach a steady state.

Two series of measurements were performed. The signal from HR.PHM60 was either transported to the CTF3 streak camera laboratory for time domain measurements with a 20 GHz sampling oscilloscope, or filtered in the detection system and transported to the CTF3 control room for analysis in the frequency domain.

3.1 Time domain measurements

In order to visualize directly the time structure of the bunch trains circulating in the ring, the signals from HR.PHM60 were transported to the CTF3 streak camera laboratory through a 50 Ω RF cable, with a total length of 10 m. There, the signals were read on the sampling oscilloscope, triggered by the streak camera timing system.

In a first step, no bunch train combination was performed and the time structure of one single pulse was studied. Figure 23 shows that not only the signal produced by the 6-7 ns long bunch train is detected. Some reflections may occur in the pick-up itself but, most likely, some wakefields also induce a significant amount of signal in the pick-up. When electron bunches travel inside the beam pipe, various waveguide modes may be excited along their path and then propagate together with the bunch train. Since these modes can be produced at many locations in the ring and since they propagate with different velocities, some may be detected at the same time as the bunch train (in that case, the wakefields induce aperiodic ringing between the signals produced by the bunches), while others may arrive at the pick-up location up to tens of ns after the passage of the bunch train.

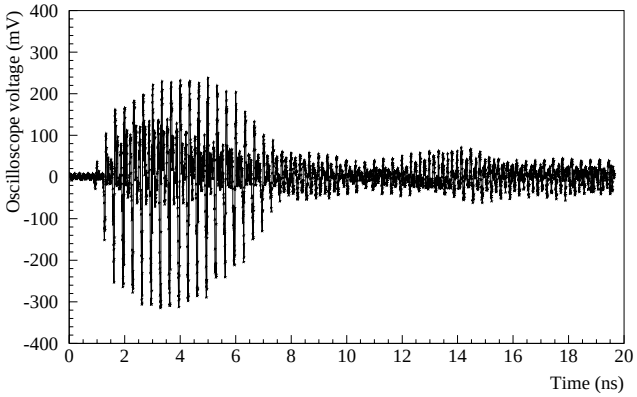

Figure 23: Time structure of the signal induced in the pick-up by the passage of one bunch train in the CTF3 isochronous ring. The 6-7 ns long pulse is clearly visible on the left-hand side, while some signal induced by the wakefields can be observed on the right-hand side.

The same measurement was then performed with a different timing of the streak camera trigger, in order to visualize the waveform obtained after the bunch frequency multiplication with a factor five. Figure 24 shows how the bunch trains are interleaved in order to form a pulse with a bunch spacing about five times smaller than originally. Since the source does not deliver perfectly identical pulses, variations in length may occur from one bunch train to the other. Hence, the longitudinal overlap between the bunch trains is not perfect and the bunch frequency multiplication only occurs in the core of the final pulse. The bunch trains may also have slightly different orbits and/or transverse sizes because of the betatron oscillations, depending on the number of turns they perform in the ring after their injection. This leads to variations in the amplitude of the transverse fields from one bunch train to the other: in the pulse obtained after the combination, different bunch trains do not induce the same amount of signal.

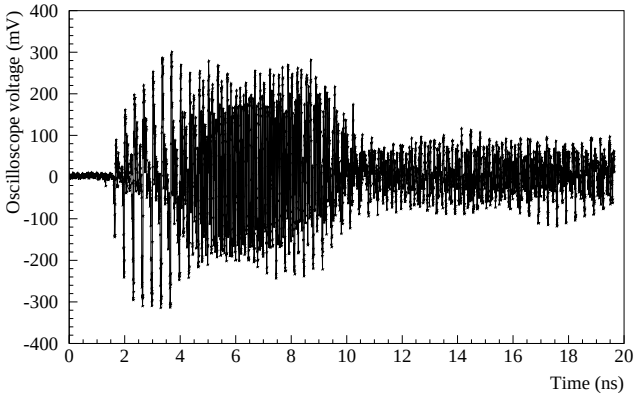

Figure 24: Same as Figure 23, but after combination of five bunch trains.

A Fourier Transform analysis of the time signal was performed at each step of the bunch train combination. As expected, it showed that only the harmonics of 3 GHz are found in the frequency spectrum. Also, we noticed that the power associated to the 15 GHz harmonic clearly increases while the bunch trains are combined. However, the repartition of the power between the various harmonics is not uniform along the bunch train. In particular, only the core of the pulse has an almost pure 15 GHz structure, while all harmonics of 3 GHz can still be found at the edges of the pulse. The fact that the bunch trains do not perfectly overlap is the main reason for this effect. Finally, by treating separately the pulse and the tail, we noticed that the power spectrum of the signal induced by the wakefields contains the same harmonics as the signal induced by the bunches themselves, although not with the same amplitudes. For all harmonics, the power found in the first 8 ns of the waveform, i.e. in the pulse, is about one order of magnitude larger than the power found in the last 8 ns of the waveform, i.e. in the tail. This suggests that, in spite of the presence of wakefields, frequency domain measurements can be performed in order to monitor the bunch frequency multiplication, because the main contribution to the power spectrum of the pulse comes from the bunch train itself. However, the wakefields travelling between the bunches do contribute to the power spectrum as well. Frequency domain measurements do not allow any discrimination between the signal induced by the wakefields and the signal induced by the bunches, which may be a serious limitation when one wants to perform accurate measurements.

3.2 Frequency domain measurements

In order to directly study the evolution of the beam frequency spectrum during the bunch train combination, the signal coming out from HR.PHM60 was first filtered in the read-out electronics and then analysed with a fast multi-channel digital oscilloscope. When performing the measurements with HR.PHM60, the charge per bunch was found to be about 0.06 nC. The bunch length, which was measured with the streak camera, is between 7 and 12 ps fwhm (in the following, we will consider an average fwhm length of 10 ps). The beam transverse position in HR.PHM60 was derived from the positions measured in HR.UMA55 and HR.UMA61 and we found $x = -1.0 \pm 1.0$ mm and $y = -1.6 \pm 0.8$ mm, for the horizontal and vertical directions, respectively. MAFIA simulations were performed in order to estimate the power level of the 6.6 ns long pulse coming out from HR.PHM60, for each harmonic of interest and at each stage of the bunch train combination, see Table 1.

Step	Power level for each harmonic f_i				
	9 GHz	12 GHz	15 GHz	18 GHz	21 GHz
1	-22.1 dBm	-18.6 dBm	-19.5 dBm	-20.7 dBm	-18.9 dBm
2	-26.3 dBm	-14.4 dBm	-13.5 dBm	-16.5 dBm	-23.1 dBm
3	-26.3 dBm	-14.4 dBm	-10.0 dBm	-16.5 dBm	-23.1 dBm
4	-22.1 dBm	-18.6 dBm	-7.5 dBm	-20.7 dBm	-18.9 dBm
5	-	-	-5.6 dBm	-	-

Table 1: Expected power levels at the output of HR.PHM60, for the five harmonics of interest, at each step of the bunch frequency multiplication with a factor five. The charge per bunch is 0.06 nC, the fwhm bunch length is 10 ps and the beam transverse positions are $x = -1.0$ mm and $y = -1.6$ mm.

An RF synthetizer driven by a DC pulse generator was then used to inject 6.6 ns long RF signals into the detection system, at each frequency of interest and with the power levels that were estimated with MAFIA. The output waveforms were stored for further comparison with the signals coming directly from HR.PHM60.

Figure 25 shows the HR.PHM60 signals, as measured by the oscilloscope at each step of the bunch train combination. The distance between the pulses is 420 ns, as expected. The shape of the pulses is often distorted because of the contribution of the wakefields. The open circles correspond to the peak amplitude of the output signal which is obtained when 6.6 ns long RF pulses are injected into the detection system, with the power levels of Table 1. At 15 GHz, the signal amplitude clearly increases each time a new bunch train is injected into the ring and, at the end of the bunch frequency multiplication, most of the power is found in the 15 GHz harmonic, as expected. However, other channels also receive some signal. The corresponding pattern is not consistent with a phase error at injection. It is thus probably due to the fact that the longitudinal overlap between the five bunch trains is not perfect (the bunch frequency multiplication mainly occurs in the core of the final pulse). This may also partly explain the discrepancies between the expected and measured signal amplitudes. Another reason for these discrepancies, and for the distorsion of the pulses, may be the presence of wakefields between the bunches (note that, depending on their phase, they can induce either an increase or a decrease of the output signal).

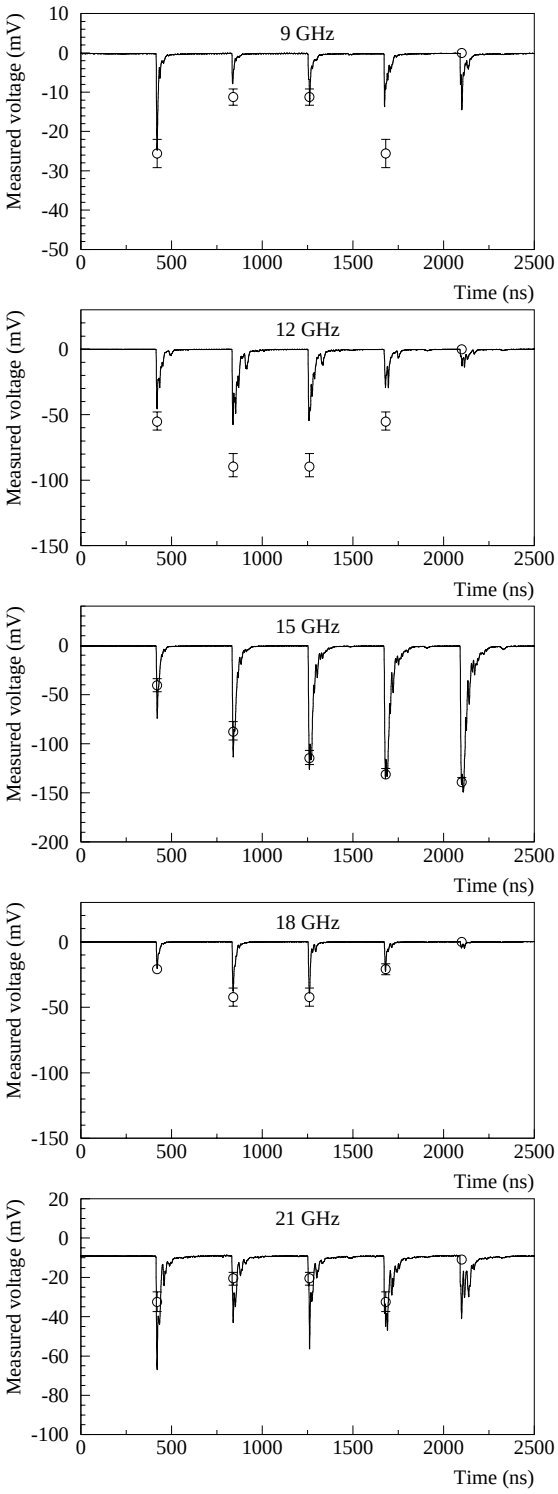

Figure 25: Signals from HR.PHM60, as measured downstream of the instrumentation, while a bunch frequency multiplication with a factor five occurs. The open circles show the expected amplitude for 20 bunches with a charge of 0.06 nC, a fwhm length is 10 ps and travelling at $x = -1.0$ mm and $y = -1.6$ mm. The error bars account for the uncertainties on the measurement of the beam transverse position and of the bunch length.

The same measurement was also performed with a bunch frequency multiplication factor four and leads to the same conclusion: we successfully commissioned an instrument aimed at monitoring the combination of bunch trains in the CTF3 isochronous ring, however with two limitations: the first one is the fact that the time extension of the bunch trains is smaller than the rise time of the electronics, which makes it difficult to measure accurately the absolute power level contained in each harmonic. The second limitation is the presence of waveguide modes propagating in the beam pipe, in the wake of the electron bunches, and leading to a distorsion of the signal from the monitor.

4 Conclusion

In this note, we have reported on the third operation period of the CTF3 Preliminary Phase in 2002. New RF deflectors with a larger aperture than the ones used before were installed in the isochronous ring. After having optimized the optics and defined a setting-up procedure, the bunch train combination process was successfully demonstrated with a factor four and five. Streak camera measurements showed that the bunch length remained constant over several turns in the ring and was comparable to what was measured at the end of the linac. Bunch-to-bunch variations in intensity and transverse position were observed and could be linked to pulse-to-pulse variations in charge, length, energy and longitudinal profile. We also noticed the presence of bunch-to-bunch distance variations and we could demonstrate that they are related to the non-achromaticity of the ring at the streak camera observation point. These bunch-to-bunch distance variations were indeed constant in the regions of the ring with a zero-dispersion (injection and extraction). Therefore, this effect was not a major limitation for the bunch train combination and it should not affect the possible use of the combined beam for the production of high-frequency power. Finally, new instrumentation aimed at monitoring the bunch frequency multiplication was successfully commissioned, with two limitations however: the fact that the time extension of the bunch trains was smaller than the rise time of the read-out electronics, and the presence of waveguide modes propagating in the wake of the electron bunches.

The dismantling of the CTF3 Preliminary Phase started after this last operation period, in order to make room for the next stages of the CTF3 facility.

Acknowledgements

The authors wish to thank D. Alesini, F. Marcellini, M. Preger, S. Quaglia and A. Stella (INFN-LNF, Frascati) for their participation in this CTF3 Preliminary Phase operation period.

The research of A. Ferrari has been supported by a Marie Curie Fellowship of the European Community Programme ”Improving Human Research Potentiel and the Socio-economic Knowledge Base” under contract number HPMF-CT-2000-00865.

References

[1] R. Corsini, A. Ferrari, L. Rinolfi, P. Royer and F. Tecker, ”Report on the second operation period of the CTF3 Preliminary Phase in 2002, 27 May - 23 August”, CTF3 note 052, PS/AE note 2002-194.

[2] R. Corsini, B. Dupuy, A. Ferrari, L. Rinolfi, P. Royer and F. Tecker, ”Commissioning of the CLIC Test Facility 3 Preliminary Phase in 2001”, CLIC note 507, CERN-PS note 2002-005 (AE).

[3] R. Corsini, A. Ferrari, L. Rinolfi, P. Royer and F. Tecker, ”Report on the operation of the CTF3 Preliminary Phase, 8 April - 24 May 2002”, CTF3 note 049, PS/AE note 2002-141.

[4] A. Ferrari and A. Rydberg, ”Design of a bunch phase monitor for the CTF3 preliminary phase”, CTF3 note 046, PS/AE note 2002-061.

[5] Computer Simulation Technology, ”Mafia Release 4.106”, CST Darmstadt, Germany.

[6] J. Durand, T. Tardy and R. Trabelsi, ”A miniature ultrahigh vacuum feedthrough usable from DC to 20 GHz”, PS/LP/96-09 (tech), EST/96-03.